A TRMM-CALIBRATED INFRARED RAINFALL ALGORITHM APPLIED OVER BRAZIL

A. J. Negri[*1], L. Xu[2] , and R. F. Adler[1]

[1]Laboratory for Atmospheres

NASA/Goddard Space Flight Center, Greenbelt, MD 20771

[2] Dept. of Hydrology and Water Resources, U. Arizona, Tucson, AZ 85721

Journal of Geophysical Research

Submitted to the special issue on LBA

12/2/00

* Corresponding author address: Andrew J. Negri,
NASA/GSFC, Code 912, Greenbelt, MD 20771;
email: negri@agnes.gsfc.nasa.gov

ABSTRACT

The development of a satellite infrared technique for estimating convective and stratiform rainfall and its application in studying the diurnal variability of rainfall in Amazonia are presented. The Convective-Stratiform Technique, calibrated by coincident, physically retrieved rain rates from the TRMM Microwave Imager (TMI), is applied during January to April 1999 over northern South America. The diurnal cycle of rainfall, as well as the division between convective and stratiform rainfall is presented. Results compare well (a one-hour lag) with the diurnal cycle derived from TOGA radar-estimated rainfall in Rondonia. The satellite estimates reveal that the convective rain constitutes, in the mean, 24% of the rain area while accounting for 67% of the rain volume. The effects of geography (rivers, lakes, coasts) and topography on the diurnal cycle of convection are examined. In particular, the Amazon River, downstream of Manaus, is shown to both enhance early morning rainfall and inhibit afternoon convection. Monthly estimates from this technique, dubbed CST/TMI, are verified over a dense rain gage network in the state of Ceara, in northeast Brazil. The CST/TMI showed a high bias equal to +33% of the gage mean, indicating that possibly the TMI estimates alone are also high. The root mean square difference (after removal of the bias) equaled 36.6% of the gage mean. The correlation coefficient was 0.77 based on 72 station-months.

1. Introduction

In this paper, we present the application of and results from a satellite infrared (IR) technique for estimating rainfall over northern South America. Our objectives are to examine the diurnal variability of rainfall and to investigate the relative contributions from the convective and stratiform components. There is a paucity of hourly-reporting rainfall stations in northern South America in general and the Amazon Basin in particular. Hence, most of the literature describing the diurnal cycle of rainfall in this region has necessarily used satellite observations as a proxy for rainfall. One notable exception is *Kousky* (1980), who examined the diurnal cycle of rainfall in northeast Brazil from 10 years of gage observations. Estimates from IR-only methods include *Meisner and Arkin* (1987), who found a pronounced maximum in IR cloudiness at 1800 LT over the interior of summertime South America. *Janowiak and Arkin* (1991) examined the period 1986-1989 for seasonal and interannual variations in estimated rainfall. *Horel et al.* (1989) looked at 15 years of twice-daily out-going longwave radiation measurements to describe the annual cycle of convection in the Amazon Basin. More recently, *Garreaud and Wallace* (1997) examined 9 years of high spatial resolution IR data to define the diurnal march of deep convection over the tropical Americas and surrounding waters.

With the launch of the Special Sensor Microwave Imager (SSM/I) in 1987, microwave (MW) algorithms were developed and applied. Examples include *Negri et al.* (1994), a 5-year climatology of warm-season tropical rainfall, and *Negri et al.* (2000), and a 10-year climatology over northern South America. Using four SSM/I observations per day, they showed dramatic

differences in afternoon versus morning rain estimates. Methodology using a combination of MW and IR include *Huffman et al.* (1995, 1997) who made global, monthly rain estimates from a merger of IR, MW, gage and models. Other techniques adjust existing IR techniques by the MW measurements. Examples include *Negri et al.* (1993), a 3-year, warm-season study over Mexico, and *Xu et al.* (1999, 2000) who adjust the GOES Precipitation Index (GPI) by MW observations from SSM/I in an attempt to improve monthly rainfall estimates. Recently, the Passive Microwave and Infrared Algorithm (MIRA) [*Todd et al.,* 2000] attempts to estimate small-scale rainfall. In the forerunner of the research described in this paper, *Anagnostou et al.* (1999) trained IR observations with three months of SSM/I observations to deduce the diurnal cycle of rainfall over northern South America.

In this study, we apply the Convective-Stratiform Technique (CST) of *Adler and Negri,* [1988]. The parameters of the original technique were recalibrated using coincident rainfall estimates derived from the Tropical Rain Measuring Mission (TRMM) Microwave Imager (TMI) and GOES IR (11 μm) observations. Henceforth, we refer to this new technique as the CST/TMI.

2.0 Data and Methodology

In this study, we apply the Convective-Stratiform Technique (CST) of *Adler and Negri,* [1988]. In short, the CST locates, in an array of IR data, all local minima in the brightness temperature field. After an empirical screening to remove thin, non-raining cirrus, the remaining

minima are assumed centers of convective rain. A stratiform rain assignment, based on the mode temperature of each cloud system, completes the rain estimation. The parameters of the original technique were recalibrated using coincident rainfall estimates derived from the application of the Goddard Profiling (GPROF) algorithm to TMI brightness temperatures [*Kummerow and Giglio*, 1994; *Kummerow et al.*, 1996]. We use an improved algorithm for convective/stratiform division in the GPROF as described by *Olson et al.*, [2000].

Over northern South America, the GOES-east observes every 30 min; therefore, we were able to match a TMI image with an IR image within a 15 min window. Calibration was performed over land only, from 12N to 18S and from 82W to 34W. The TMI rain estimates contain the distribution of total surface rainfall as well as the classification of convective and stratiform rain. The matched data (165 TRMM overpasses) are in the period from January to April, 1999, the first two months of which coincide with the period of the Large-Scale Biosphere-Atmosphere (LBA) experiment in Brazil.

The goal of the recalibration is to determine parameters so that the CST will be able to reproduce the total rain volume, total rain area, and the TMI-observed division between convective and stratiform rain. We adjust the CST on a statistical basis, over the 4-month calibration period, without explicit constraints on instantaneous rain estimates. The recalibration takes the following form:

a) determination of convective cores using a discriminant analysis. This is based on the identification of points of local IR temperature minimum (T_{min}) and the computation of the deviation of the T_{min} from the background temperature (defined as the average temperature of the eight surrounding pixels). Figure 1 shows the analysis of T_{min} in the 2-dimensional space defined by IR temperature and the deviation of the T_{min} from the background. Points are defined by the corresponding TMI-retrieved rain rate as either convective (C) or non-convective (N). Plotted data represents a 1% random subset of the total dataset used to derive the discriminant line. T_{min} points above and to the left of the discriminant lines are deemed convective. The resultant discriminant lines are defined by:

$$1.25 \cdot T_{min} - 3.16 \cdot \text{Deviation} \leq 254.7 \text{ and Deviation} \leq 2.23$$

b) determination of the convective rain area assigned to each T_{min}. This is based on the computation of α, the constant of proportionality between the total convective area in the TMI estimates and the parameter $\Sigma(T_{cloud} - T_{min})$. For a given convective T_{min}, $\alpha \cdot (T_{cloud} - T_{min})$ is the number of pixels to which we assign a convective rain rate centered on the T_{min}. In this study T_{cloud} is a constant set to 253 K, a commonly used threshold for convective clouds. Based on the rain area determined from the TRMM convective area estimates, $\alpha = 0.61$. For $T_{min} = 203$ for example, 32 pixels (4 by 4 km) would be assigned the convective rain rate.

c) determination of the mean convective rain rate. We set the convective rain rate equal to the conditional rain rate of the TMI/GPROF estimates, namely 18.9 mm h^{-1}. This allows the

total convective rain volume derived from CST /TMI to equal that calculated from the TMI alone.

d) determination of the threshold temperature to define the stratiform rain area. We choose a threshold such that the total cloud area colder than this threshold (excluding those pixels already assigned convective rain) is equal to the stratiform rain area derived by TMI/GPROF. This threshold, calculating using cumulative area matching, was found to be 219 K.

e) determination of the mean stratiform rain rate. As in the case of determining the convective mean rain rate, the conditional TMI/GPROF stratiform rain rate of 2.6 mm h^{-1} was used. This forces the total stratiform rain volume from CST/TMI to equal that of the TMI alone, integrated over the 4-month calibration period.

In summary, the CST/TMI finds local IR minima, decides if they are convective features, then assigns a rain area and rainrate based on the TMI calibration parameters. A stratiform rain area is then defined, and a lower rain rate is assigned to those cloud pixels colder than the stratiform IR threshold and not previously assigned convective rain. We have chosen two rain rates to make the technique simple and efficient. An example of the instantaneous application of this technique is shown in Figure 2. The four panels indicate (clockwise from the upper left): a GOES IR image of southwestern Brazil; the CST/TMI rainfall estimate; the rain rate from the

TRMM radar algorithm 2A25; and the GPROF-retrieved rain rate applied to the TMI brightness temperatures. For reference, the outline of the TMI swath appears on all images.

3. Results

3.1 The Diurnal Cycle in the TOGA Radar Area

Rain estimates over northern South America (12N to 18S, 82W to 34W) were made from 30 min interval GOES data for the period January-April, 1999. The first two months of this period coincided with the LBA experiment in Rondonia, (southwestern Brazil). TOGA radar data provided a comparison between the mean radar rain rates and convective/stratiform division with those estimated by the CST. The satellite estimates were matched in both time (5 min) and space (accounting for bad and missing data) to the gage-calibrated radar estimates [Anagnoustou et al., 2000]. Figure 3 (left) displays the mean rain rate (mm h^{-1}) from the TOGA radar at 1 km height for the period 7 Jan to 28 Feb 1999. The asterisks mark the location of the four main clusters of rain gages. Problems with beam blockage and ground clutter along several azimuths necessitated the creation of a quality control mask (Figure 3, right). This mask represents the frequency of occurrence of rainfall in the interval 7-13%. (Higher than 13% was determined to be ground clutter; lower than 7% was beam blockage). Instantaneous radar estimates were averaged only within the confines of this mask, and it is apparent that problems remain with the radar data.

Figure 4 shows the diurnal variation of four rain parameters during the experiment period of 7 Jan to 28 Feb 1999. The upper left panel of the figure displays the unconditional rain rate for

the CST/TMI estimates (green), TOGA radar (red) and rain gages (blue). The upper right panel shows the percent of the radar area covered by rain greater than 1 mm h^{-1}. The lower left panel tracks the variation of the convective rain rate (the percent of the rain volume due to convective rain). Finally, the lower right panel reveals the variation of the percent of the rain area due to convective rain. The satellite estimates of the mean rain rate (top left) are in good agreement with both the radar and gages. They lag the radar (and gage) estimates by one hour, essentially missing the earliest stages of convection. By comparison, results using a simple threshold method (the GOES Precipitation Index or GPI, not plotted) showed a three-hour lag in the maximum rainfall. The mean values of the satellite, gage and radar estimates are, respectively, 0.35, 0.35 and 0.43 mm h^{-1}. Compared to the radar estimates, the CST/TMI overestimates the fractional convective rain volume (bottom left) by a factor of 1.36, while underestimating the fractional convective area (bottom right) by a factor of 1.57. An underestimation of the total rain area by a factor of 1.52 is also noted. Despite the biases, the phase of all four of the satellite-estimated parameters seems to well represent (within an hour of the maximum), the phase of the radar-derived rainfall. The satellite estimates reveal that the convective rain constitutes, in the mean, 24% of the rain area while accounting for 67% of the rain volume.

3.2 Results for Northern South America

Figure 5 shows the application of the CST/TMI to 30 min interval data from January-April 1999 over the northern portion of South America. Results (in mm h^{-1}) are binned into hourly

categories and adjusted for local time (3 zones). The final panel displays the mean rain rate for the entire 4-month period. Among the interesting features revealed in this presentation are:

- The development of afternoon (12 – 20 LT) squall lines along the Northeast Brazilian coast. Such squall lines were studied by *Garstang et al.*, [1990].
- A morning maximum and afternoon minimum in rainfall along the Amazon River east of Manaus. This is described in more detail in the next section;
- A morning rain maximum in the Gulf of Panama, no doubt in response to a land breeze along the highly convergent coastline;
- The onset of deep convection in the Amazon Basin around 13 LT, maximizing at 15-16 LT;
- A late evening (23 LT) to early-morning (05 LT) maximum along the eastern slopes of the southern Andes Mountains, possibly the result of a mountain/valley circulation;
- An afternoon (13-18 LT) maximum along the western slopes of the southern Andes.

Many more small-scale features are revealed when these 24 images are viewed in time-sequence. A QuickTime™ movie of this sequence is available by contacting the first author. An alternate method of displaying these hourly data is shown in Figure 6, the arithmetic difference of the CST/TMI estimates at 18 LT and 06 LT. These times correspond with the overpass times of the Special Sensor Microwave Imager (SSM/I). Areas with an afternoon maximum are displayed in yellow to red shades, while areas of morning maximum appear blue to purple. In an

effort to validate these results, we present Figure 7, the estimated rainfall difference (18 –06 LT) derived from the application of the GPROF algorithm to SSM/I brightness temperatures from the F13 DMSP satellite. Spatial resolution is 0.5° and the temporal sampling is about 20 observations/month at both 18 and 06 LT. Note the similarity of features, particularly along the coasts and rivers, which lend credibility to the IR estimates.

3.3 Effects of the Amazon River on the Rainfall

Figure 8 is a blow-up of the mean hourly estimates in Figure 5, along the confluence of the Negro and Solimões Rivers near Manaus, Amazonia, Brazil. Here we find a late-evening (00 LT) rainfall maximum that elongates and moves westward along the river until about 10 LT. Convection begins by 12 LT, and there is a pronounced minimum in rainfall along the river from about 15 to 18 LT.

Figure 9 is a time/latitude display of the mean estimated rain rate for January-April, 1999 (left) and January-April, 2000 (right) for a cross-section through the Amazon River at 56W. The mean position of the Amazon River at this longitude is noted. Downstream of where the Negro and Solimões Rivers merge, we find an early morning (3 LT) maximum *along* the river. Rainfall *avoids* the river in the afternoon (12 LT and later). The river seems to be generating a land/river circulation, which enhances early morning rainfall but inhibits afternoon rainfall along the river. Such phenomenon have been studied by *Oliveira & Fitzjarrald*, [1993]. The pattern is

duplicated a year later, January-April, 2000 (right), demonstrating the repeatability of the phenomenon.

3.4 Diurnal curves for other regions

Buoyed by the success of the technique in an area with ground-truth, we examine the diurnal variation of rainfall in other regions. In Figure 10, we display a time series of the estimated total, convective and stratiform rain rates (mm/h) for three regions of interest. In the region encompassing much of the Amazon Basin (top), peak convective rainfall occurs at 15-16 LT. The convective rainfall comprises about 74% of the total rainfall at the time of the maximum, and 67% overall. The stratiform estimates lag the convective by two hours. Estimates for a smaller subset of the Amazon Basin, along the Amazon R. (downstream of the confluence of the Negro and Solimões Rivers) are shown in the middle panel of Fig. 3. A pronounced rainfall maximum at 3 LT is noted. The bottom panel of Fig. 3 shows the diurnal curve for the northeast Brazil area, where coastal squall lines form almost daily. The peak estimated rainfall is 1.3 mm/h at 17 LT, and at the maximum, has a percentage of convective rainfall of 65%. The stratiform lags the convective by 2 h.

3.5 Monthly Verification in the State of Ceara, Brazil

Figure 11 is an example of the monthly rainfall (April 2000) in the state of Ceara in northeast Brazil. Monthly rainfall is highest along the coast, and tapers off as one moves inland, until

higher elevations are reached in the southern part of the state. This gage data was averaged in the nine 1° squares outlined in the figure for comparison to the area-averaged CST/TMI estimates. Figure 12 shows a scatterplot of the estimates versus the gages for the wet season for two years (January-April, 1999-2000). Standard deviations of the mean gage rainfall for the nine grid squares in Fig. 11 are plotted to demonstrate the high spatial variability of rainfall. The CST/TMI shows a bias (+33% of the gage mean). The root mean square difference after removal of the bias (RMSD-br) is 36.6% of the gage mean, but the technique is not specifically calibrated in this region. We are encouraged by the high correlation coefficient of 0.77.

4. Conclusions

In this paper, we have presented results from a satellite infrared technique for estimating rainfall over northern South America. The parameters of the technique were calibrated using coincident rainfall estimates derived from the application of the GPROF algorithm to TRMM Microwave Imager brightness temperatures. Our objectives were to examine the diurnal variability of rainfall at high space and time resolution, and to investigate the relative contributions from the convective and stratiform components. TOGA radar data during the LBA experiment provided radar ground truth for both the CST rainfall and convective/stratiform estimates.

The diurnal cycle of rainfall in the LBA radar area was constructed. The peak satellite-estimated rainfall lagged the radar by one hour. Identification of the onset of convection was the

primary cause of this lag. Estimates of the division of rainfall into convective and stratiform components were also accomplished. The phase of these components agreed with the radar estimates, though the convective volume (area) was overestimated (underestimated). The satellite estimates revealed that the convective rain constitutes, in the mean, 24% of the rain area while accounting for 67% of the rain volume. Local circulations were found to play a major role in modulating the rainfall and its diurnal cycle. These included land/sea circulations (notably along the northeast Brazilian coast and in the Gulf of Panama), mountain/valley circulations (along the Andes Mountains), and circulations associated with the presence of rivers. This last category was examined in detail along the Amazon R. east of Manaus. There we found an early morning rainfall maximum *along* the river (3 LT at 56W). Rainfall *avoids* the river in the afternoon (12 LT and later. The width of the river seems to be generating a land/river circulation that enhances early morning rainfall but inhibits afternoon rainfall.

Verification of the monthly CST/TMI results was performed using rain gages in the northeast Brazilian state of Ceara. The CST/TMI showed a high bias equal to +33% of the gage mean. The root mean square difference after removal of the bias was 36.6% of the gage mean. We were encouraged by the high correlation coefficient of 0.77 for a technique is not specifically calibrated in this region.

Perhaps the most important future application of this technique may be assessing the impact of deforestation on the both the rainfall and it's diurnal cycle. We intend to run the CST/TMI for a full year, and compare monthly and seasonal total and hourly rain estimates with maps of

forested and deforested regions of Amazonia. We hope that circulations like that described over the Amazon River will exist over these regions, and manifest themselves in the satellite rainfall estimates. A second application involves the application of this technique to global, high-resolution, geosynchronous IR data sets (*Janowiak et al.*, 2001).

Acknowledgements. This research was funded by the Atmospheric Dynamics and Thermodynamics Program at NASA Headquarters. The continued support of Dr. Ramesh Kakar is appreciated. We would like to thank Geraldo Ferriera of FUNCEME (Meteorology and Water Resources Foundation of Ceara, Brazil) for providing the raingage data. We also would like to thank Dr. Emmanouil Anagnostou and Dr. Carlos Morales of the University of Connecticut for processing and providing the gage-calibrated TOGA radar estimates.

References

Adler, R.F. and A.J.Negri, 1988: A satellite infrared technique to estimate tropical convective and stratiform rainfall. *J. Appl. Meteor., 27*, 30-51.

Anagnostou, E. N., A. J. Negri, and R. F. Adler, 1999: A satellite infrared technique for diurnal rainfall variability studies. *J. Geophys. Res., 104*, 31,477-31,488.

Anagnostou, E. and C. Morales, 2000: Rainfall Estimation from TOGA Radar Observations during TRMM-LBA Field Campaign. AGU (Fall meeting-Atmospheric Sciences).

Garreaud, R. D. and J. M. Wallace, 1997: The diurnal march of convective cloudiness over the Americas. *Mon. Wea. Rev., 125*, 3157-3171.

Garstang, M., H. L. Massie, Jr., J. Halverson, S. Greco, and J. Scala, 1990: Amazon coastal squall lines. Part I: Structure and kinematics. *Mon. Wea. Rev., 122*, 608-622.

Horel, J. D., A. N. Hahmann, and J. E. Geisler, 1989: An investigation of the annual cycle of convective activity over the Tropical Americas. *J. Climate, 2*, 1388-1403.

Huffman, G. J., R. F. Adler, B. Rudolf, U. Schneider, and P. R. Keehn, 1995: Global precipitation estimates based on a technique for combining satellite-based estimates, rain gauge analysis, and NWP model precipitation information. *J. Climate*, *8*, 1284-1295.

Huffman, G. J., R. F. Adler, P. Arkin, A. Chang, R. Ferraro, A. Gruber, J. Janowiak, A. McNab, B. Rudolf, and U. Schneider, 1997: The Global Precipitation Climatology Project (GPCP) combined precipitation dataset. *Bull. Amer. Meteor. Soc.*, *78*, 5-20.

Janowiak, J. E. and P. A. Arkin, 1991: Rainfall variations in the tropics during 1986-1989 as estimated from observations of cloud-top temperature. *J. Geophys. Res.*, *96*, 3359-3373.

Janowiak, J. E., Y. Yarosh, and R. J. Joyce, 2001: A real-time global half-hourly pixel-resolution infrared data set and its applications. *Bull. Amer. Meteor. Soc.*, *82*, (in press).

Kousky, V. E., 1980: Diurnal rainfall variation in Northeast Brazil. *Mon. Wea. Rev.*, *108*, 488-498.

Kummerow, C. and L. Giglio, 1994: A passive microwave technique for estimating rainfall and vertical structure information from space, Part I: algorithm description. *J. Appl. Meteor.*, *33*, 3-18.

Kummerow, C., W. S. Olson, and L. Giglio, 1996: A simplified scheme for obtaining precipitation and vertical hydrometeor profiles from passive microwave sensors. *IEEE Trans. Geosci. Remote Sensing*, *34*, 1213-1232.

Meisner, B. N. and P. A. Arkin, 1987: Spatial and annual variations in the diurnal cycle of large-scale tropical convective cloudiness and precipitation. *Mon. Wea. Rev.*, *115*, 2009-2032.

Negri, A. J., R. F. Adler, R. A. Maddox, K. W. Howard, and P. R. Keehn, 1993: A regional rainfall climatology over Mexico and the southwest United States derived from passive microwave and geosynchronous infrared data. *J. Climate*, *6*, 2144-2161.

Negri, A. J., R. F. Adler, E. J. Nelkin, and G. J. Huffman, 1994: Regional rainfall climatologies derived from Special Sensor Microwave Imager (SSM/I) data. *Bull. Amer. Meteor. Soc.*, *75*, 1165-1182.

Negri, A. J., E. N. Anagnostou, and R. F. Adler, 2000: A 10-year climatology of Amazonian rainfall derived from passive microwave satellite observations, *J. Appl. Meteor.*, *39*, 42-56.

Oliveira and D. Fitzjarrald, 1993: The Amazon river breeze and the local boundary layer: I. Observations. *Boundary Layer Met. 63*, 141-162.

Olson, W., Y. Hong, C.D. Kummerow, and J. Turk, 2000: A texture-polarization method for estimating convective/stratiform precipitation area coverage from passive microwave radiometer data, *J. Appl. Meteor.*, (submitted).

Todd, M. C., C. Kidd, D. Kniveton, and T. J. Bellerby, 2000: A combined satellite infrared and passive microwave technique for estimation of small scale rainfall. *J. Atmos. Oceanic Technol., 17,* (in press).

Xu, L., X. Gao, S. Sorooshian, P. Arkin, and B. Imam, 1999: A microwave infrared threshold technique to improve the GOES Precipitation Index. *J. Appl. Meteor., 38*, 569-579.

Xu, L., X. Gao, S. Sorooshian, and B. Imam, 2000: Parameter estimation of GOES precipitation index at different calibration time scales. *J. Geophys. Res., 105*, 20,131-20,143.

Figure Captions

Figure 1. Discriminant analysis of IR temperature minima (T_{min}) in the 2-dimensional space defined by IR brightness temperature and the deviation of the T_{min} from the background. Points are defined by the corresponding TMI-retrieved rain rate as either convective (C) or non-convective (N) rain. Plotted data represents a 1% random subset of the total dataset used to derive the discriminant line.

Figure 2. An example of the application of the CST/TMI to one IR image. The outline of the TMI swath is overlain on all images.

(Upper left): GOES IR image of southwestern Brazil scanned at 2358 GMT 22 Jan 1999;

(Upper right): CST/TMI rainfall estimate. Convective cores (green) have a mean rain rate of 18.9 mm h^{-1} while stratiform rain areas (purple) have a mean rain rate of 2.6 mm h^{-1};

(Lower left): Rain rate retrieved by application of the GPROF algorithm to the TMI microwave brightness temperatures. Overpass occurred 7 min after the time of the GOES image;

(Lower right): Rain rate from the TRMM radar algorithm 2A25.

Figure 3. TOGA radar at 1 km height for the period 7 Jan to 28 Feb 1999. The asterisks mark the locations of the four main clusters of rain gages.

(Left): Mean rain rate (mm h^{-1})

(Right): Quality control mask applied to account for missing or bad azimuths and ground clutter.

Figure 4. The diurnal variation of four rain parameters in the period 7 Jan to 28 Feb 1999.

(Upper left): The unconditional rain rate for the CST/TMI estimates (green), TOGA radar (red) and rain gages (blue).

(Upper right): The variation the fraction of the radar area covered by rain greater than 1 mm h^{-1}).

(Lower left): The variation of the percent of the rain volume due to convective rain.

(Lower right): The variation of the percent of the rain area due to convective rain.

Figure 5. Application of the CST/TMI to 30 min interval data from January-April 1999. Results (mm h^{-1}) are binned into hourly categories and adjusted for local time (3 zones). The final panel displays the mean rain rate for the entire 4-month period.

Figure 6. The arithmetic difference of the CST/TMI estimates at 18 LT and 06 LT for the period January-April, 1999. Areas with an afternoon maximum are displayed in yellow to red shades, while areas of morning maximum appear blue to purple. Units are mm h^{-1}.

Figure 7. Same as Figure 4 except the rainfall estimates are derived from the application of the GPROF algorithm to SSM/I brightness temperatures from the F13 satellite. Spatial

resolution is 0.5° and the temporal sampling is about 20 observations/month at both 18 and 06 LT.

Figure 8. A blow-up of the mean hourly estimates (mm h^{-1}) in Figure 3, along the confluence of the Negro and Solimões Rivers near Manaus, Amazonia, Brazil.

Figure 9. A time/latitude display of the mean estimated rain rate (mm h-1) for a cross-section through the Amazon River at 56W.

(Left): January-April, 1999

(Right): January – April 2000

Figure 10. The diurnal cycle of CST/TMI rain estimates for three regions of South America:

(Top): the Amazon Basin (0-10 S, 50-75W)

(Middle): the Amazon River (2-3 S, 55-59 W)

(Bottom): the northeast Brazilian coast (2-5 S, 42-50 W)

Figure 11. Monthly gage rainfall for April 2000 in the state of Ceara in northeast Brazil.

Figure 12. Scatterplot of CST/TMI versus gage rain estimates of monthly rainfall, averaged to 1° squares, for the 8 months January-April, 1999-2000. The vertical lines with bars represent

one standard deviation of the mean gage-averaged rainfall for the nine outlined 1° squares in Figure 11.

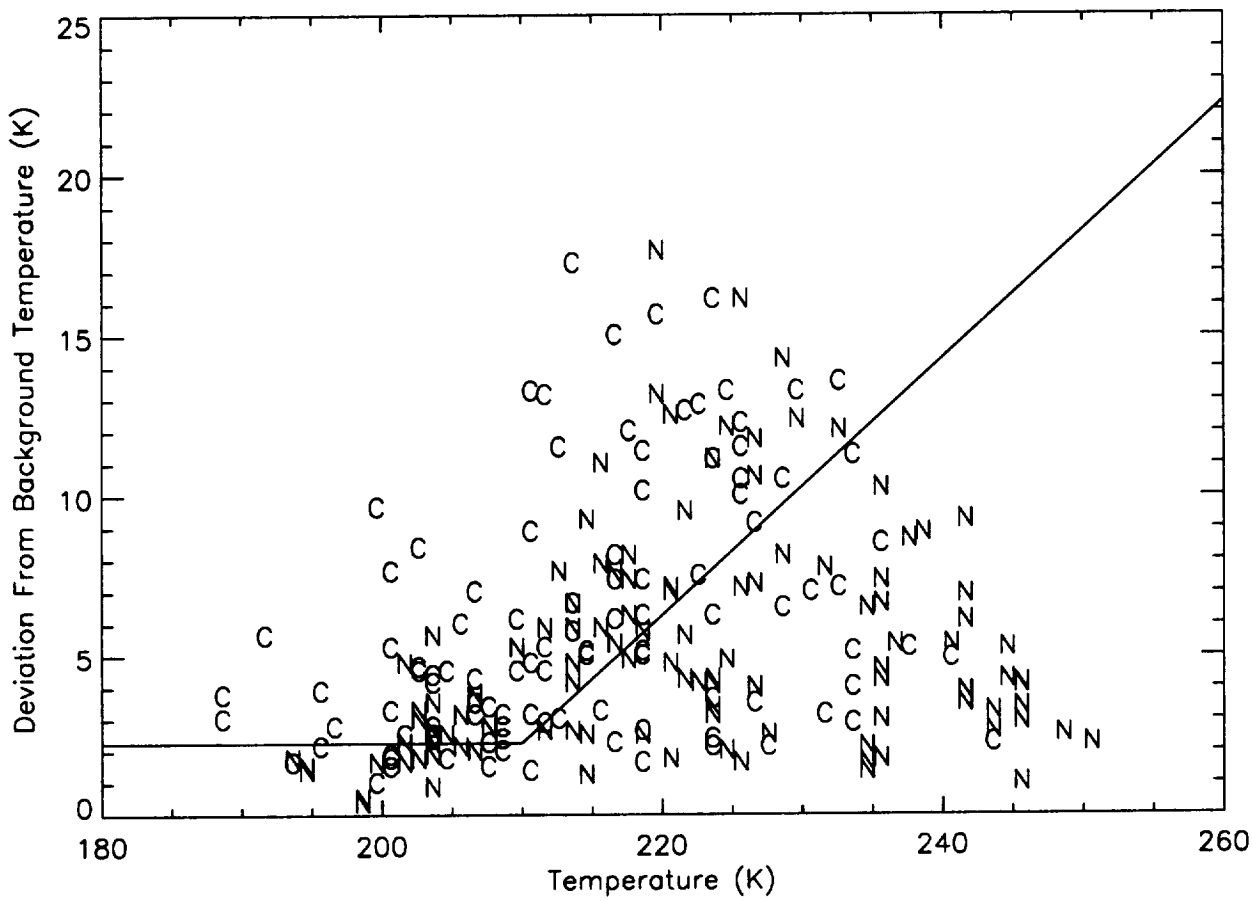
Deviation From Background Temperature (K)
25
20
15
10
5
0
180
200
220
240
260
Temperature (K)

Figure 1

GOES infrared image: 2358 GMT 22 Jan 1999

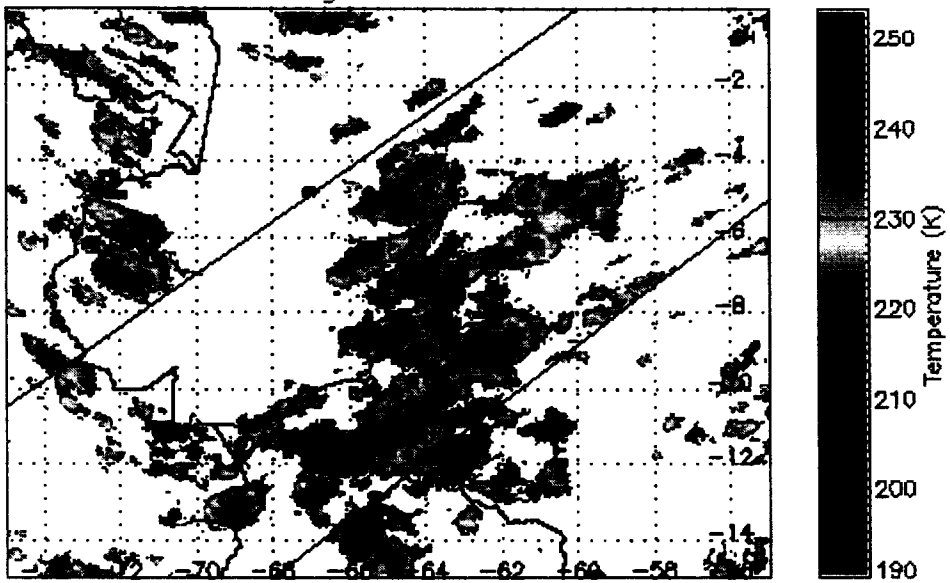

CST/TMI (IR) derived rain: 2358 GMT 22 Jan 1999

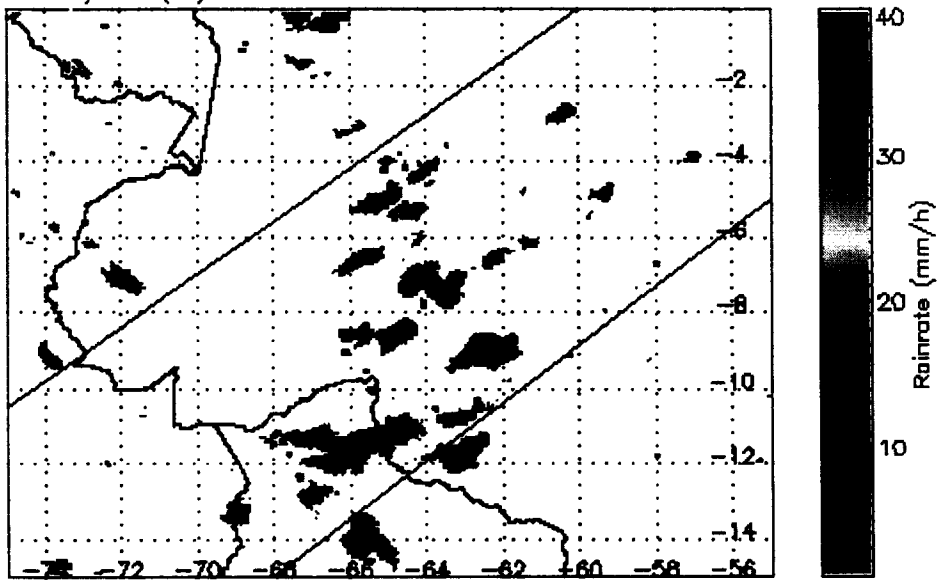

TMI/GPROF (MW) derived rain: 0005 GMT 23 Jan 1999

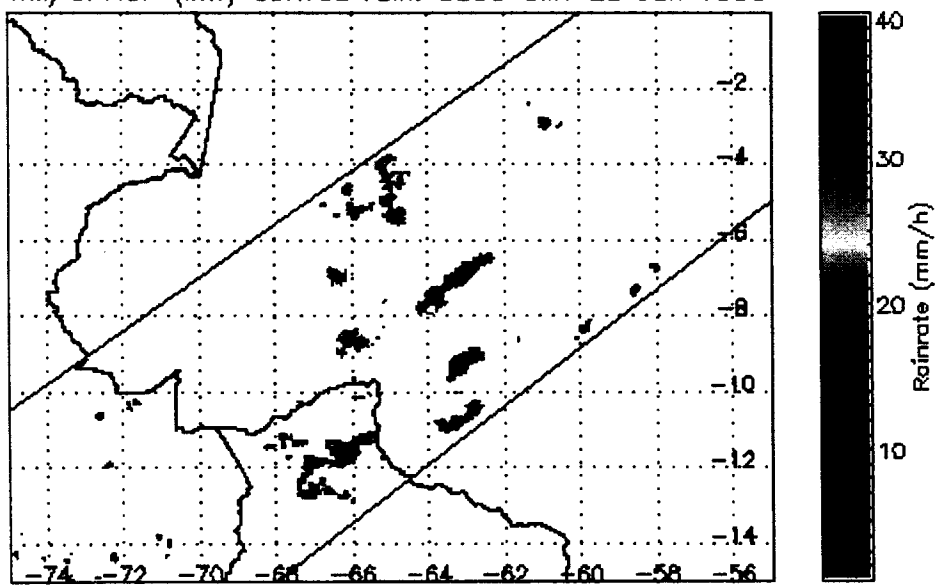

TRMM/radar derived rain: 0005 GMT 23 Jan 1999

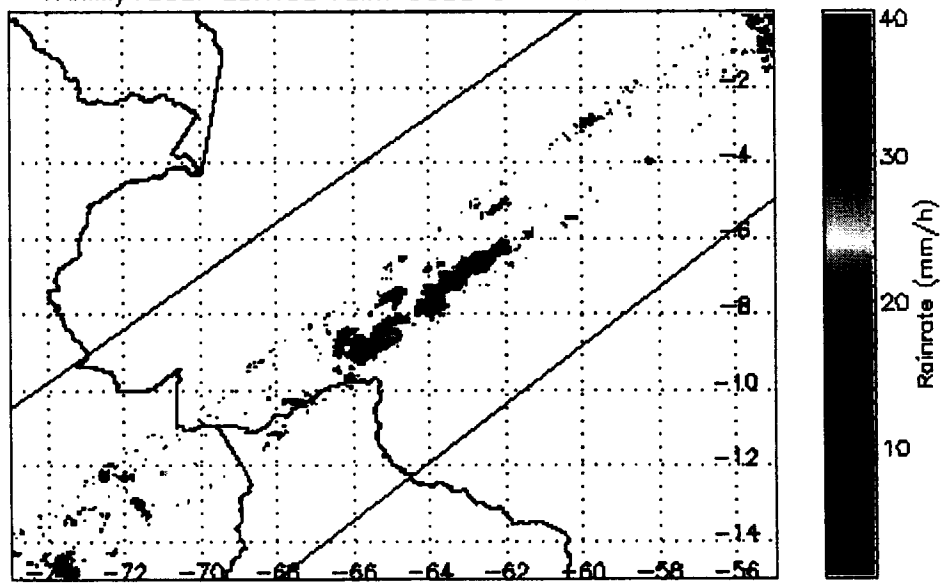

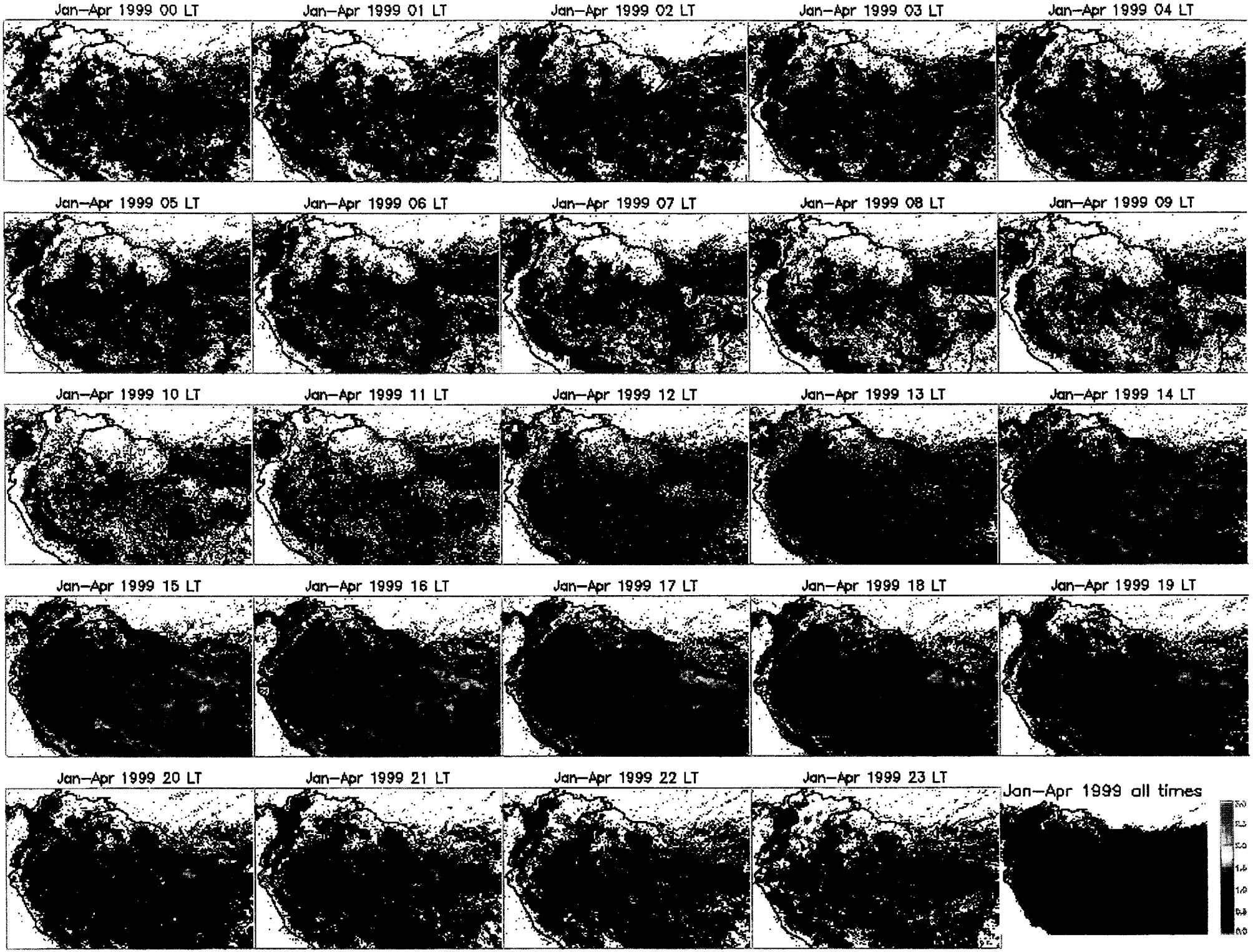
Jan–Apr 1999 00 LT
Jan–Apr 1999 01 LT
Jan–Apr 1999 02 LT
Jan–Apr 1999 03 LT
Jan–Apr 1999 04 LT
Jan–Apr 1999 05 LT
Jan–Apr 1999 06 LT
Jan–Apr 1999 07 LT
Jan–Apr 1999 08 LT
Jan–Apr 1999 09 LT
Jan–Apr 1999 10 LT
Jan–Apr 1999 11 LT
Jan–Apr 1999 12 LT
Jan–Apr 1999 13 LT
Jan–Apr 1999 14 LT
Jan–Apr 1999 15 LT
Jan–Apr 1999 16 LT
Jan–Apr 1999 17 LT
Jan–Apr 1999 18 LT
Jan–Apr 1999 19 LT
Jan–Apr 1999 20 LT
Jan–Apr 1999 21 LT
Jan–Apr 1999 22 LT
Jan–Apr 1999 23 LT
Jan–Apr 1999 all times

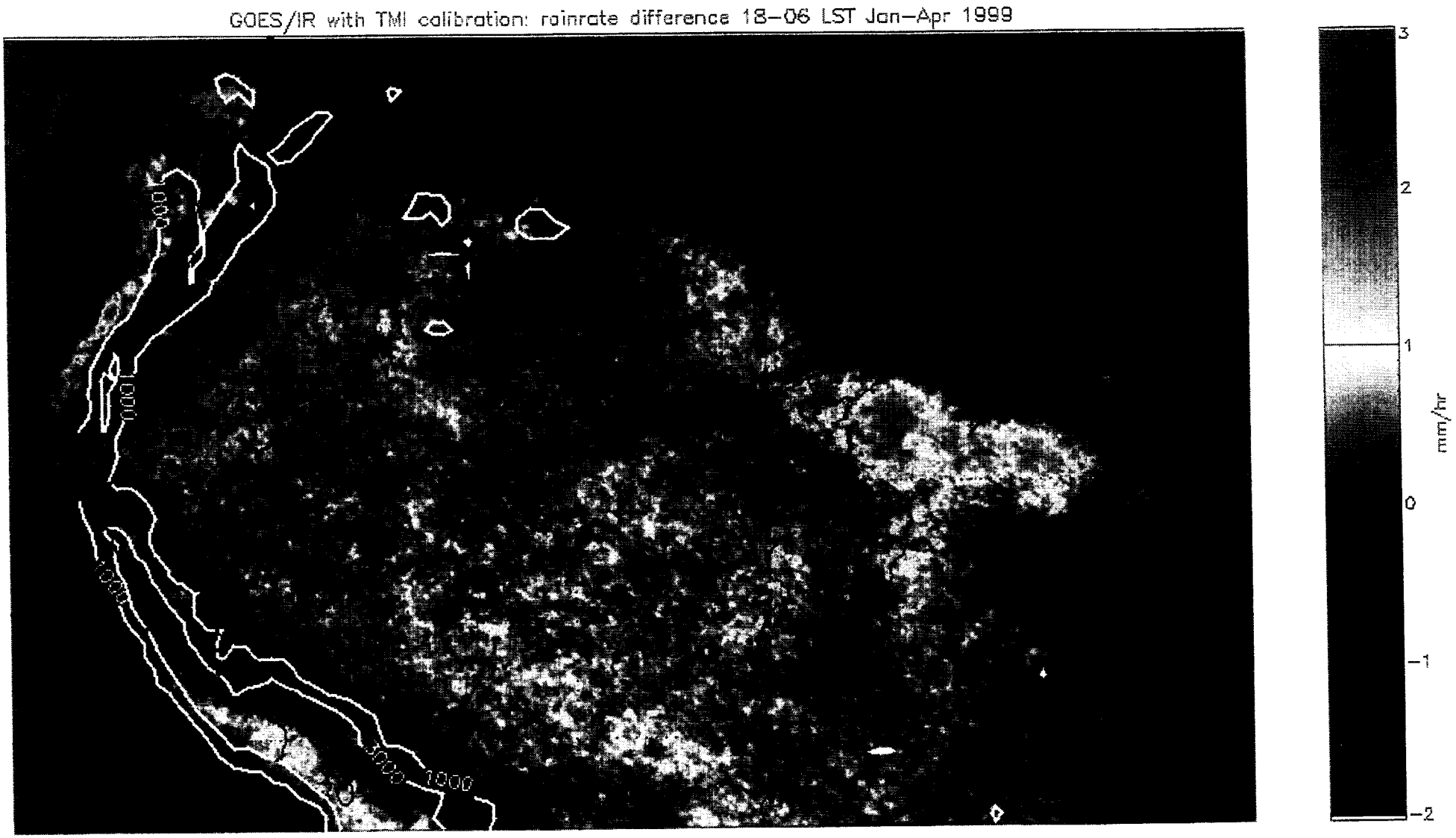
GOES/IR with TMI calibration: rainrate difference 18–06 LST Jan–Apr 1999
1000
1000
1000
1000
3
2
1
0
−1
−2
mm/hr

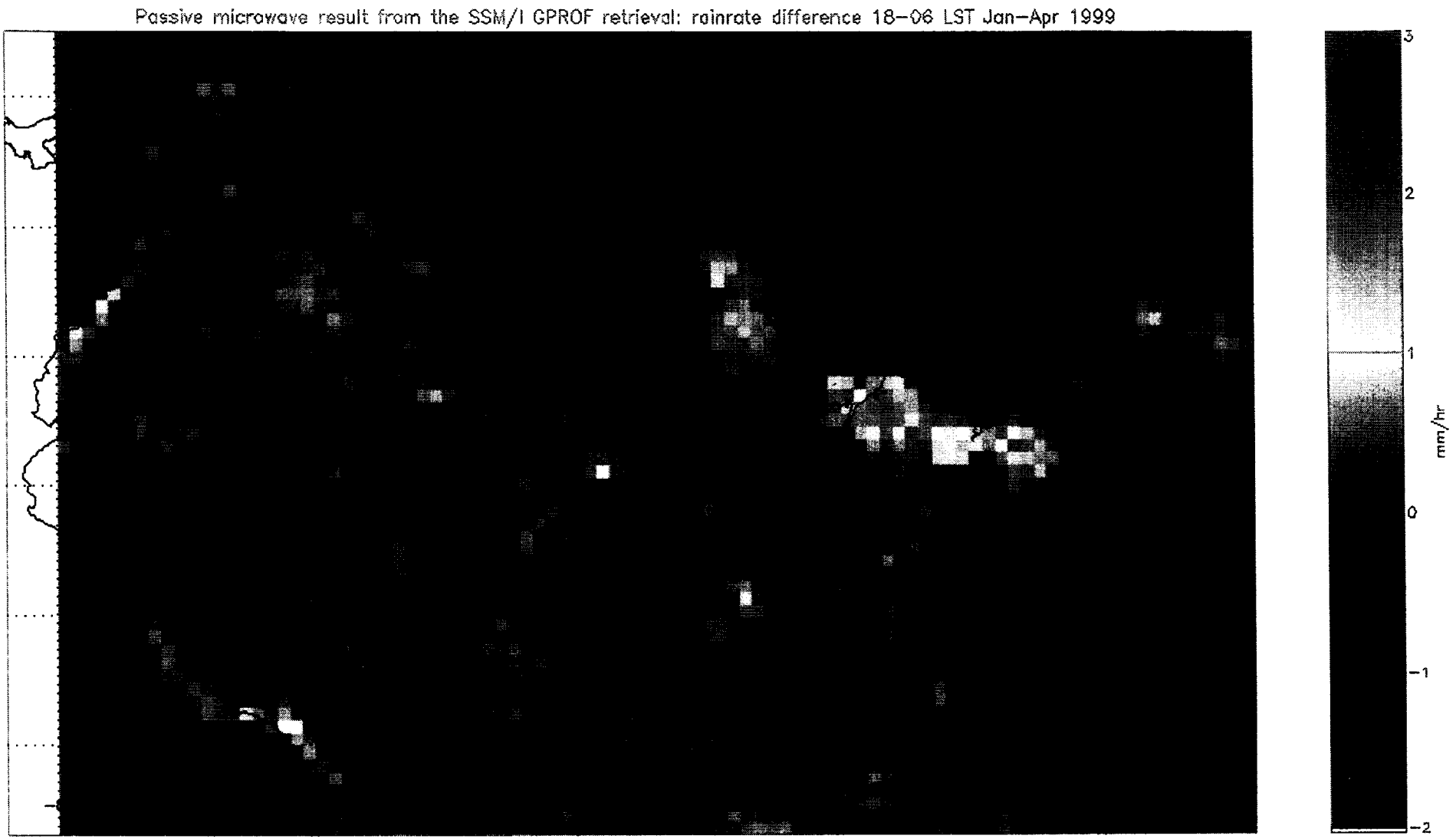
Passive microwave result from the SSM/I GPROF retrieval: rainrate difference 18–06 LST Jan–Apr 1999
3
2
1
0
−1
−2
mm/hr

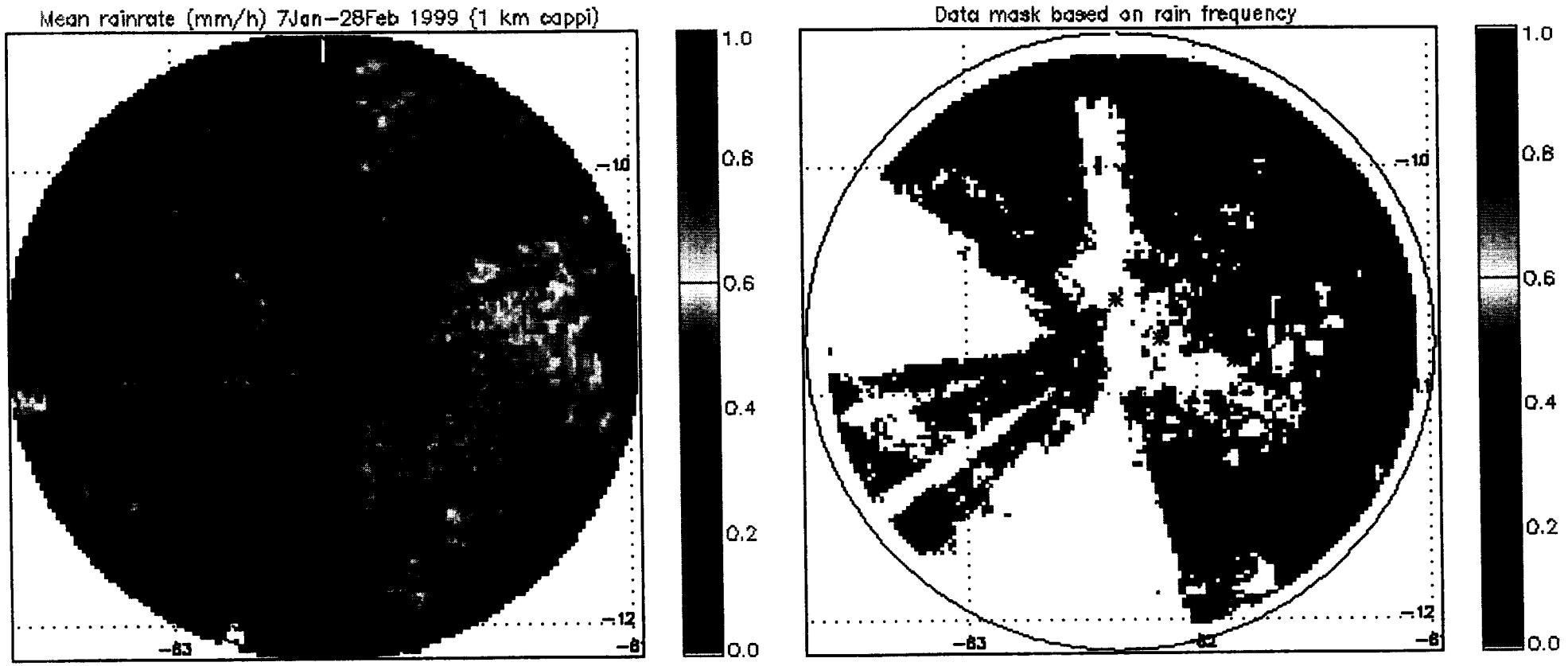
Mean rainrate (mm/h) 7Jan–28Feb 1999 (1 km cappi)
1.0
0.8
0.6
0.4
0.2
0.0
-10
-12
-83
-8
Data mask based on rain frequency
1.0
0.8
0.6
0.4
0.2
0.0
-10
-12
-83
-82
-8

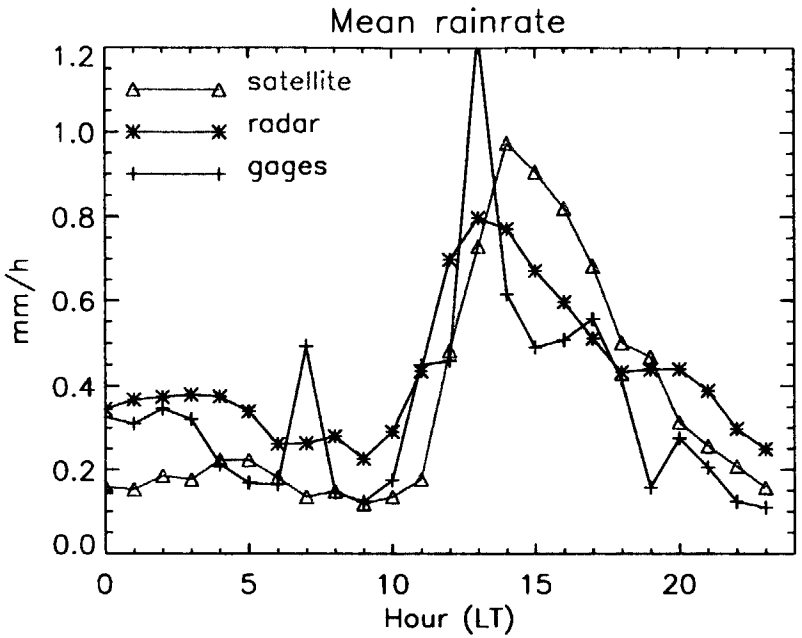
Mean rainrate
satellite
radar
gages
mm/h
Hour (LT)

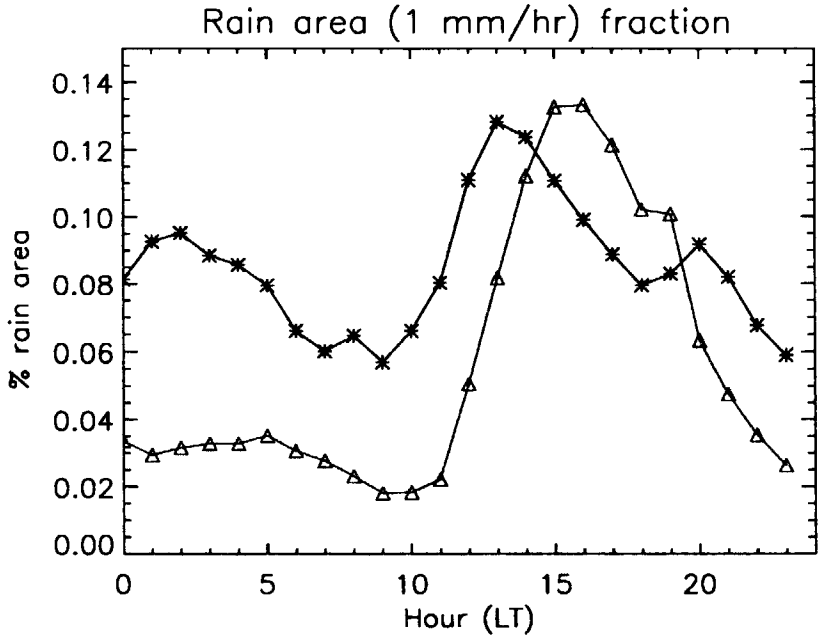
Rain area (1 mm/hr) fraction
% rain area
Hour (LT)

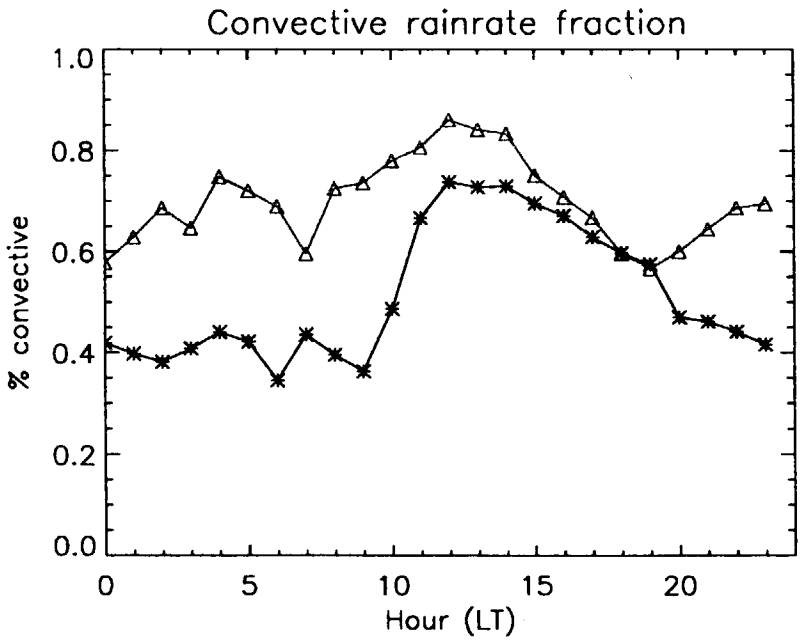
Convective rainrate fraction
% convective
Hour (LT)

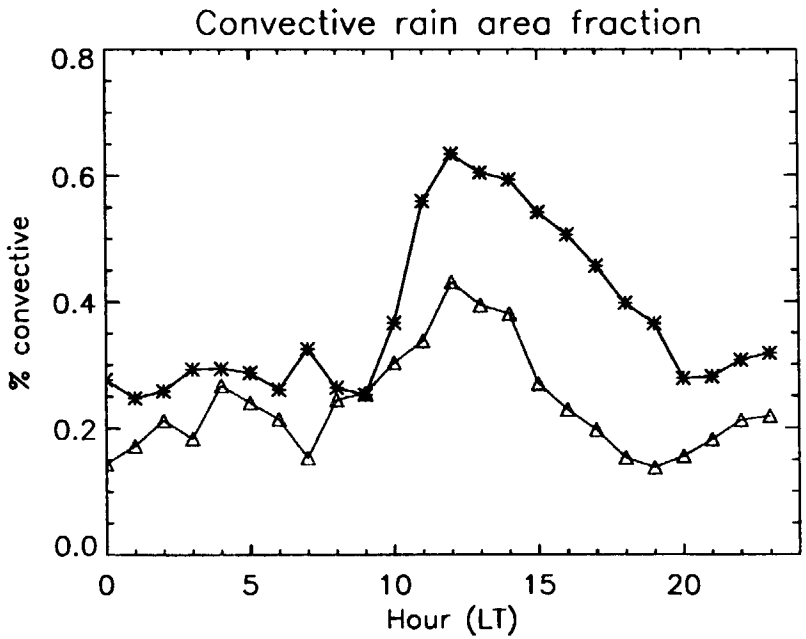
Convective rain area fraction
% convective
Hour (LT)

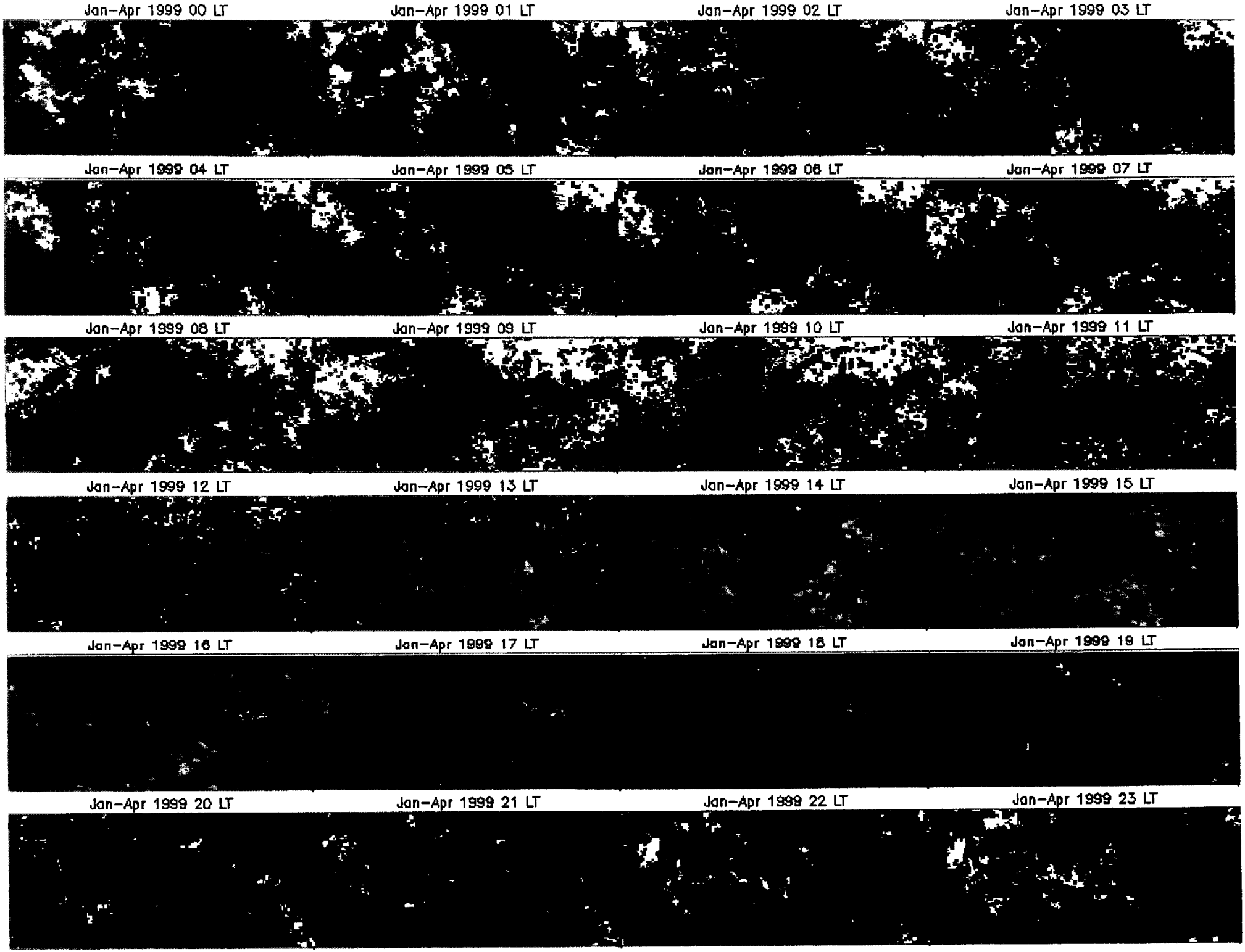
Jan–Apr 1999 00 LT
Jan–Apr 1999 01 LT
Jan–Apr 1999 02 LT
Jan–Apr 1999 03 LT
Jan–Apr 1999 04 LT
Jan–Apr 1999 05 LT
Jan–Apr 1999 06 LT
Jan–Apr 1999 07 LT
Jan–Apr 1999 08 LT
Jan–Apr 1999 09 LT
Jan–Apr 1999 10 LT
Jan–Apr 1999 11 LT
Jan–Apr 1999 12 LT
Jan–Apr 1999 13 LT
Jan–Apr 1999 14 LT
Jan–Apr 1999 15 LT
Jan–Apr 1999 16 LT
Jan–Apr 1999 17 LT
Jan–Apr 1999 18 LT
Jan–Apr 1999 19 LT
Jan–Apr 1999 20 LT
Jan–Apr 1999 21 LT
Jan–Apr 1999 22 LT
Jan–Apr 1999 23 LT

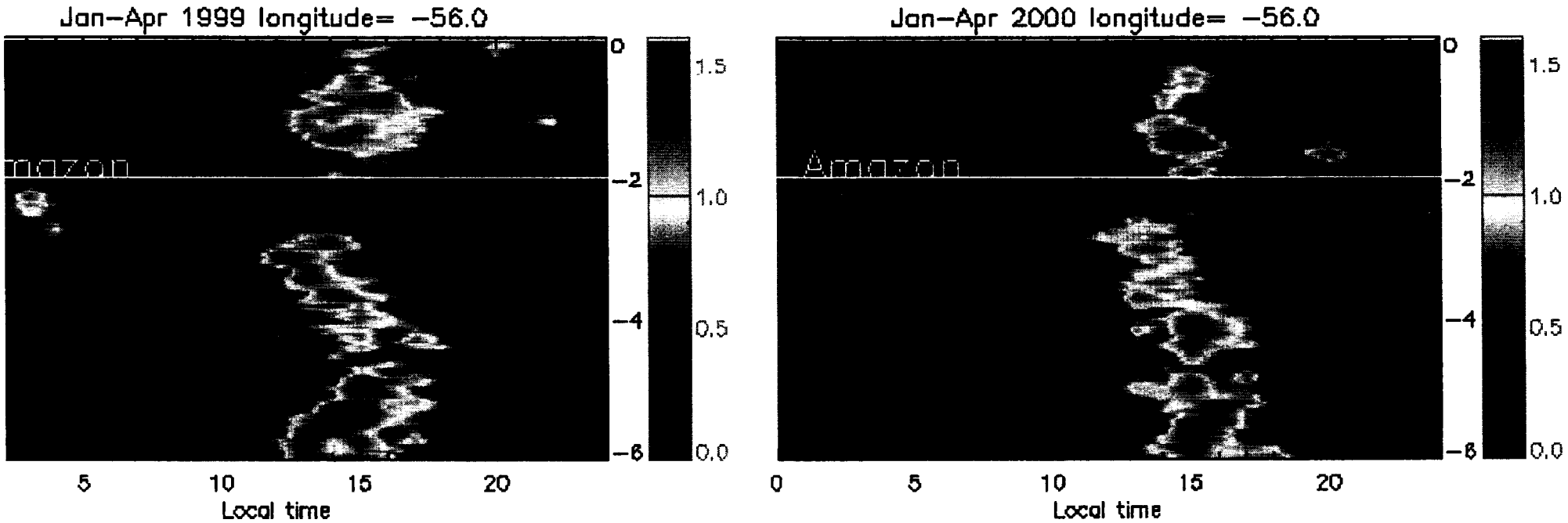
Jan–Apr 1999 longitude= –56.0
Amazon
0
–2
–4
–6
1.5
1.0
0.5
0.0
5
10
15
20
Local time
Jan–Apr 2000 longitude= –56.0
Amazon
0
–2
–4
–6
1.5
1.0
0.5
0.0
0
5
10
15
20
Local time

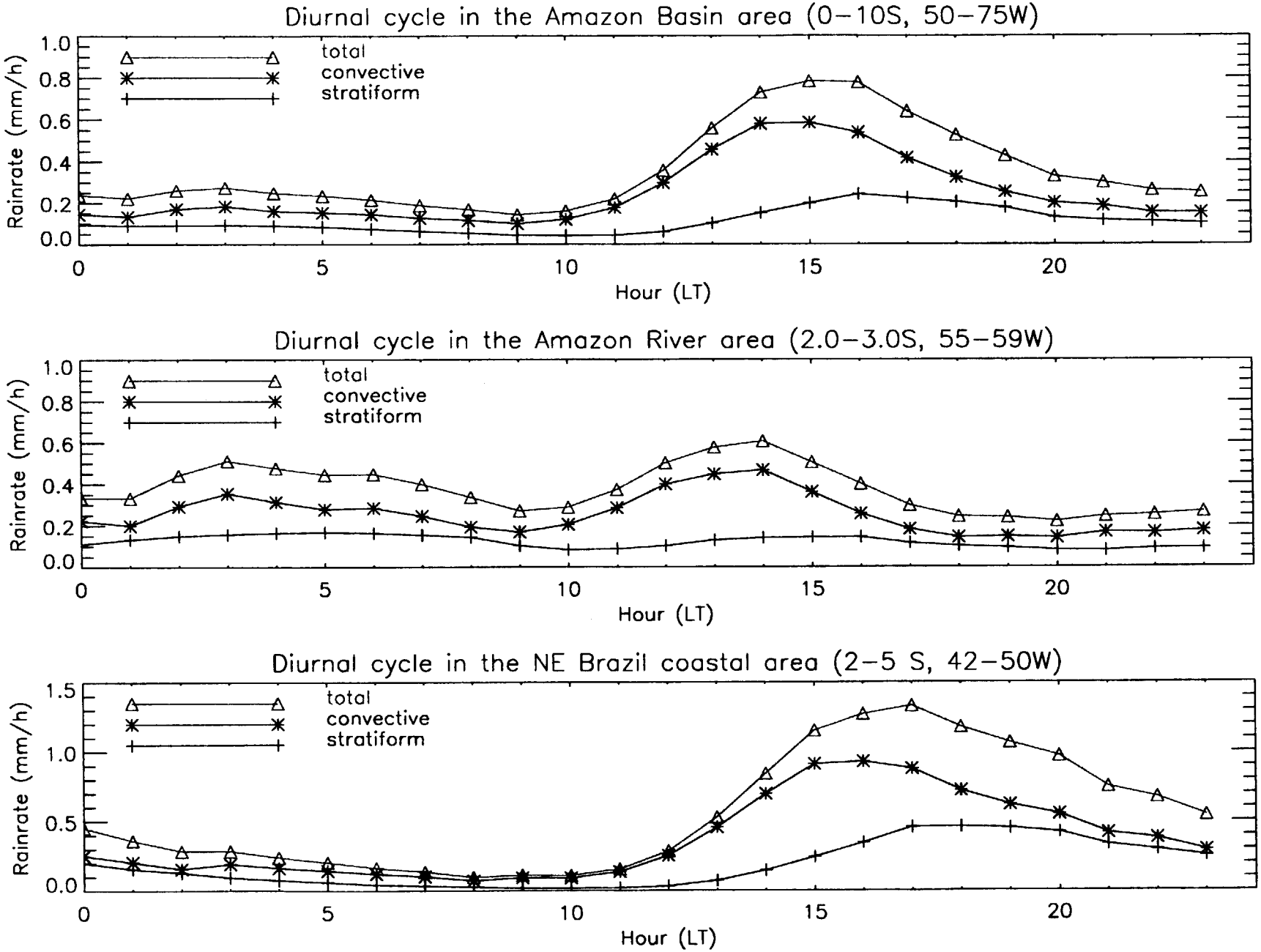
Diurnal cycle in the Amazon Basin area (0–10S, 50–75W)
total
convective
stratiform
Rainrate (mm/h)
1.0
0.8
0.6
0.4
0.2
0.0
0
5
10
15
20
Hour (LT)
Diurnal cycle in the Amazon River area (2.0–3.0S, 55–59W)
total
convective
stratiform
Rainrate (mm/h)
1.0
0.8
0.6
0.4
0.2
0.0
0
5
10
15
20
Hour (LT)
Diurnal cycle in the NE Brazil coastal area (2–5 S, 42–50W)
total
convective
stratiform
Rainrate (mm/h)
1.5
1.0
0.5
0.0
0
5
10
15
20
Hour (LT)

Figure 10

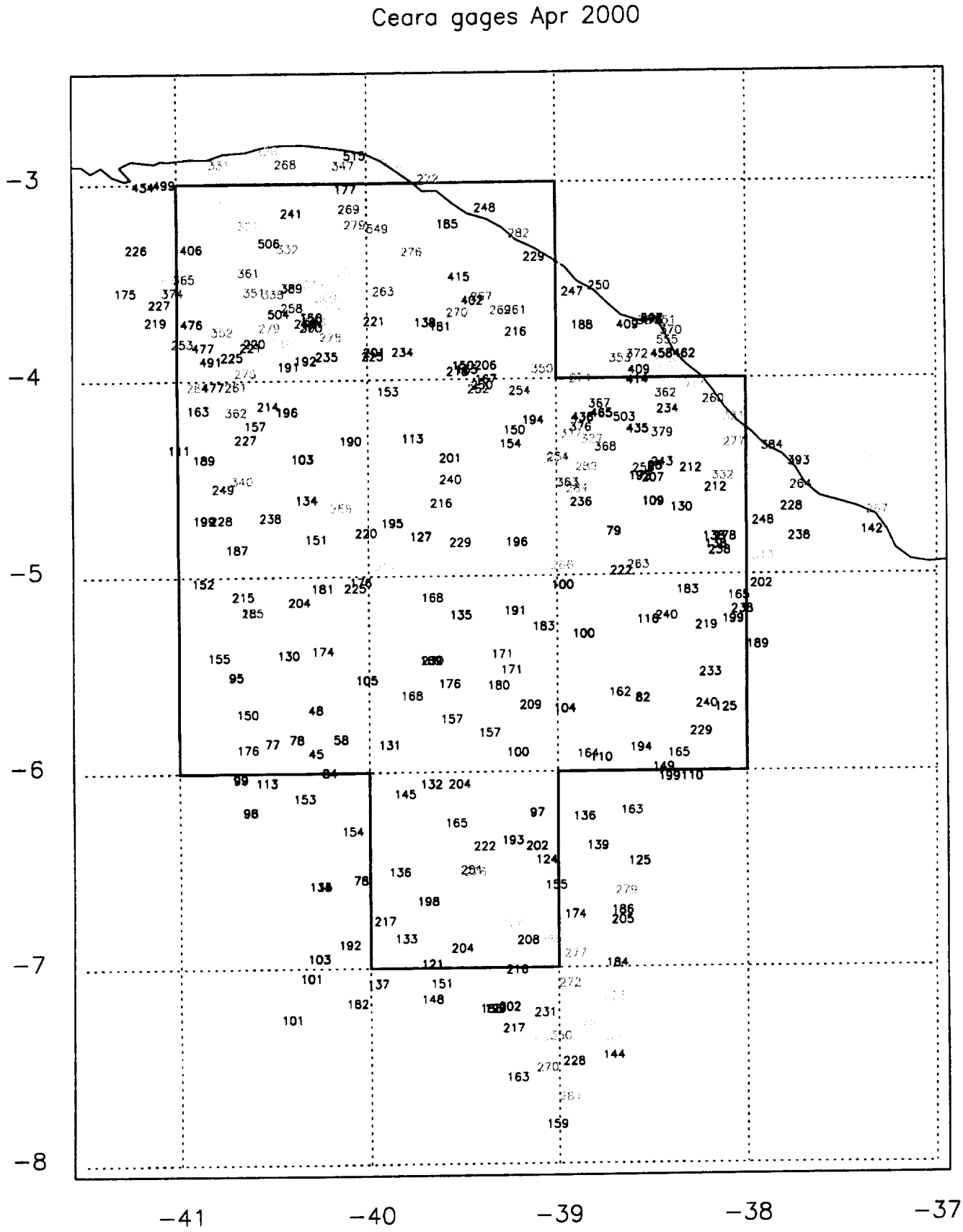

Figure 11

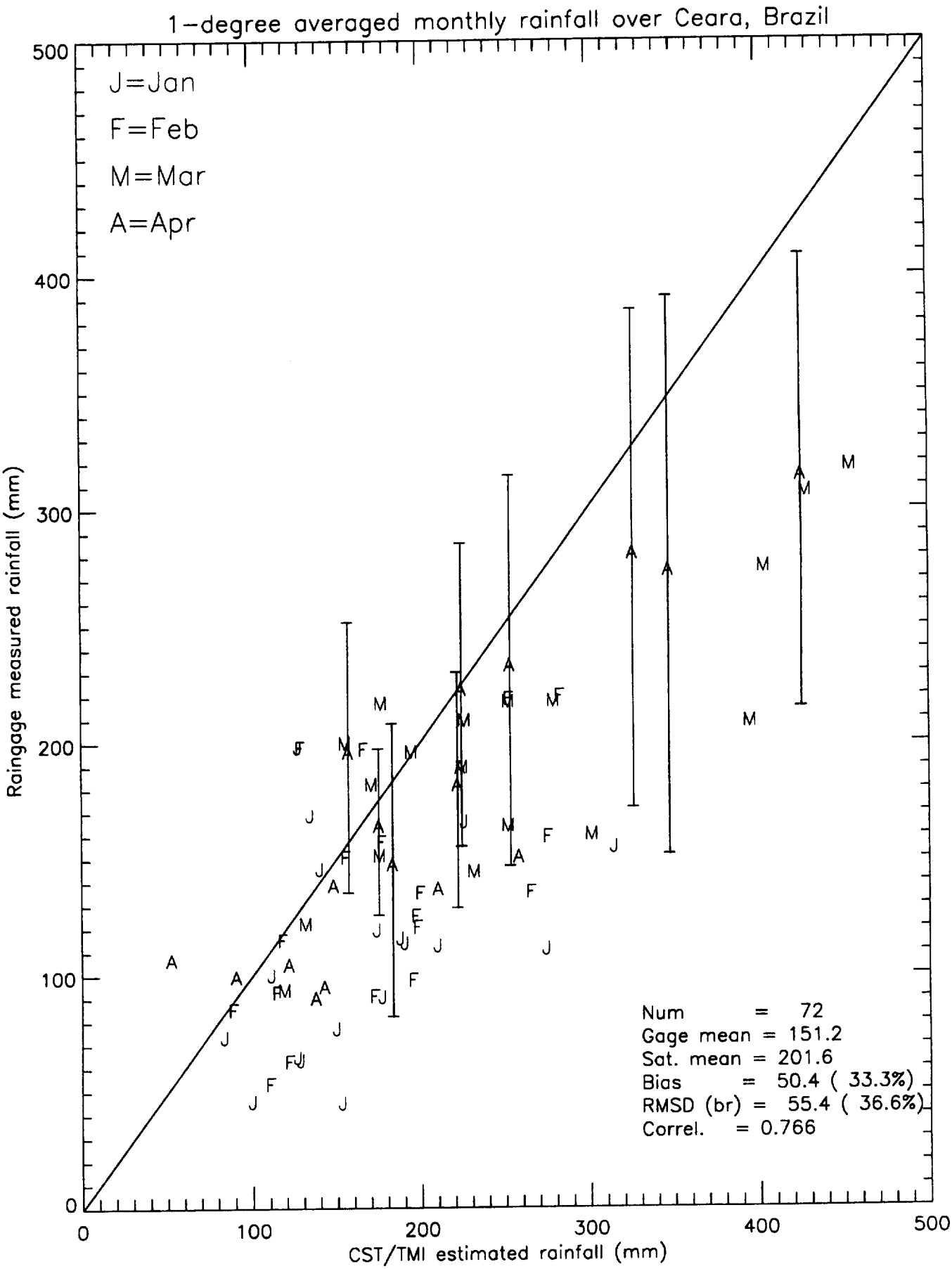
1-degree averaged monthly rainfall over Ceara, Brazil
J=Jan
F=Feb
M=Mar
A=Apr
Raingage measured rainfall (mm)
CST/TMI estimated rainfall (mm)
0
100
200
300
400
500
Num = 72
Gage mean = 151.2
Sat. mean = 201.6
Bias = 50.4 (33.3%)
RMSD (br) = 55.4 (36.6%)
Correl. = 0.766

Figure 12